GSA Data Repository 2018366

Pourteau, et al., 2018, 1.6 Ga crustal thickening along the final Nuna suture: Geology, https://doi.org/10.1130/G45198.1.

Supplementary data

ANALYTICAL METHODS

Sample preparation

The mineral separation procedure consisted of crushing fist-sized rock pieces down to cm-sized fragments using a hammer. The samples were then processed in a disk mill, rinsed with water, dried with acetone, and split into grain-sized fractions by sieving. Sieve fractions between 0.5–2.0 mm were hand panned to separate garnet and staurolite from other minerals. Samples SCG1603 and SCG1608 yielded large amounts of intact garnet porphyroblasts that could be directly handpicked from the 1–2-mm fractions, thus preventing any fractionation of garnet cores from rims due to Fe zoning (Fig. 2A–B). A second round of handpicking extracted a uniform grain size subcategory within the 1–2-mm fraction to ensure homogeneity of the dated porphyroblasts. For SCG1608, only idiomorphic porphyroblasts were used for further analysis. By contrast, sample ROB1612 did not yield good amounts of intact garnet porphyroblasts and garnet fragments were separated from the 0.5–1.0-mm fraction. Polycrystalline aggregates of low–Lu/Hf matrix phases (i.e., the ‘matrix’ aliquots) were handpicked from the different fractions depending on the samples (1–2-mm for SCG1603; 0.5–1.0 for SCG1608; 0.21–0.50 mm for ROB1612). Care was taken to select fragments devoid of garnet.

Major-element analysis

Bulk-rock powders were analysed for their major-element compositions using X-ray fluorescence (XRF) by the company Bureau Veritas (Western Australia). Mineral major-element analysis was performed on a JEOL8500F electron probe microanalyser (EPMA) at the Centre for Microscopy, Characterisation and Analysis at the University of Western Australia. Natural and synthetic minerals were used as standards. Ferrous-, and ferric iron contents of garnet and staurolite were calculated following Droop (1987).

Lu–Hf geochronology

Garnet Lu–Hf chronology was carried out at the Pacific Centre for Isotopic and Geochemical Research (PCIGR), University of British Columbia, Vancouver, following methods adopted from (Smit et al., 2010). Target garnet aliquot weight was 50–80 mg depending on the Hf concentration. Samples were mixed with a ^{176}Lu–^{180}Hf tracer solution (Lu/Hf ≈ 10), and digested through repeated addition of concentrated HF–HNO_3–$HClO_4$ and 6 N HCl, with intermittent evaporation to dryness. Matrix mineral aliquots free of garnet were mixed with a ^{176}Lu–^{180}Hf tracer solution with low Lu/Hf (~0.2) and dissolved using the same table-top dissolution technique or by adding HF:HNO_3 and placing the samples in autoclaves at 180 °C for 5 days. Total procedural blanks were processed with every group of samples and held 10 pg of Hf or less, which enabled sample/blank Hf of 1,000+ for garnet. Lutetium and hafnium were separated from their elemental matrix using cation-exchange REE–HFSE chromatography following a method adapted from (Münker et al., 2001).

Lutetium and hafnium isotopes were analysed using a Nu Instruments Plasma HR MC–ICPMS at PCIGR. For Lu, isobaric interference of ^{176}Yb on ^{176}Lu was corrected using an exponential correlation of ^{176}Yb/^{171}Yb and ^{174}Yb/^{171}Yb, calibrated through replicate analyses of NIST Yb solution standards at different concentrations (10–100 ppb; Blichert-Toft et al. 2002) and using Yb isotope abundances of (Vervoort et al., 2004). For Hf, ^{180}Ta and ^{180}W isobaric interferences on ^{180}Hf were corrected for through analysis of mass over charge corresponding to ^{181}Ta and ^{183}W and applying a Hf-based mass bias. Mass bias corrections were calculated using an exponential law and assuming $^{179}Hf/^{177}Hf = 0.7325$ (Hf, Ta, W) and $^{173}Yb/^{171}Yb = 1.1296$ (Lu, Yb). External reproducibility of $^{176}Hf/^{177}Hf$ was estimated by comparing internal and external uncertainty for replicate analyses of JMC-475 and ATI-475—isotopically identical to JMC-475 and actually made from the same metal ingots as the original JMC-475—done at concentrations that bracketed those of samples (5–50 ppb; (Bizzarro et al., 2003). The external $^{176}Hf/^{177}Hf$ reproducibility (2σ) of the replicate standard analyses was 0.25 εHf during the course of our analytical sessions. Isochrons were constructed using $\lambda^{176}Lu = 1.867 \times 10^{-11}$ yr^{-1} (Scherer et al., 2001; Söderlund et al., 2004). Uncertainties are cited at the 2σ level. The Lu–Hf data are in Table DR1.

Estimation of the metamorphic P–T evolutions

The metamorphic P–T evolution of samples SCG1608 and ROB1612 was investigated by calculating equilibrium phase diagrams and mineral composition isopleths using the software package THERIAK–DOMINO (de Capitani and Petrakakis, 2010) and an updated version of the Holland and Powell (1998) thermodynamic dataset (file tcds55_p07_rb, available at http://titan.minpet.unibas.ch/minpet/theriak/theruser.html) with the activity–composition models of White et al. (2005) recommended for Mn-rich metapelites. No solid solution was discarded. The XRF-determined bulk-rock compositions were simplified to Na_2O–CaO–K_2O–FeO–MnO–MgO–Al_2O_3–SiO_2–H_2O–TiO_2 (NCKFMASHT), assuming that all P_2O_5 was held in monazite and neglecting ferric iron. Strong compositional zoning of garnet in both modelled samples precludes that the bulk-rock composition reflects the effective bulk composition at metamorphic peak but rather at garnet growth onset. To account for chemical fractionation (especially of MnO) during prograde garnet growth and estimate peak P–T conditions, the effective bulk composition at peak conditions was recalculated in the Mn-free NCKFMASHT model system by subtracting the average composition of garnet (estimated on the basis of the profile shown in Figure DR1 and assuming spherical porphyroblasts) for all MnO, following Pourteau et al. (2018). Bulk-rock compositions used for all calculations are given in Table DR2. In all P–T calculations, H_2O was considered to be in excess.

SAMPLE DESCRIPTIONS

Phase abbreviations are from Whitney and Evans (2010). Mineral compositions are expressed as Fe# (=Fe^{2+}/(Fe^{2+}+Mg)) for all considered phases, proportions of almandine, spessartine, pyrope, and grossular end-members (xAlm, xSps, xPrp, and xGrs, respectively) for garnet, and ZnO content (in wt.%) for staurolite.

Samples SCG1603 (E140°42.085’, S20°57.162’) was collected from the eastern flank of the Snake Creek Anticline in the Soldiers Cap Domain, most eastern Mount Isa Inlier (Fig. DR1B). It is comprised of porphyroblasts of garnet (up to 2-mm across) and probably detrital monazite (up to 500 µm across) enveloped by a phyllitic matrix of muscovite, biotite, quartz, and accessory tourmaline. Prismatic porphyroblasts (Fig. 2A) consisting of randomly oriented, fine-grained muscovite, biotite, and quartz, are interpreted as former chloritoid, which formed post-foliation. Garnet, which was partially altered, contains sparse minute inclusions of ilmenite with no evident preferential orientation. The garnet porphyroblasts present slightly foliated strain shadows, and the matrix foliation is deflected at high-strain contacts (Fig. 2A). These observations suggest that garnet growth took place pre- to early foliation. Garnet shows core-to-rim decreasing xSps (16–7 %) and homogeneous xGrs (3–4 %) and Fe# = 92–93% (Fig. DR2A).

Sample SCG1608 (S20°57.097’, E140°41.791’) was collected a few hundred meters west, i.e. increasing metamorphic grade, of SCG1603 (Fig. DR1B). It is comprised of garnet (up to 1 mm across), staurolite (up to 1 cm long), and andalusite (formerly up to 4 cm long) porphyroblasts enveloped by a schistose matrix of quartz, muscovite, biotite, ilmenite, and accessory monazite, tourmaline, and apatite. Andalusite was partially overgrown by muscovite and biotite. The observed large, foliation strain shadows likely result from the replacement of andalusite during the development of the matrix. Garnet forms subhedral crystals with inclusion-rich core and inclusion-poor rims. Garnet, staurolite, and andalusite (partially overgrown by muscovite and biotite) contain inclusions of quartz and rare ilmenite that show no preferential orientation. Euhedral garnet is occasionally included in staurolite. Staurolite rims show an increasing alignment of the inclusions, which define curvilinear trails continuous with the matrix foliation. The matrix foliation is deflected around the garnet and staurolite porphyroblasts and formed non- to weakly foliated strain shadows. The strain shadows of andalusite are significantly larger and more foliated than that of garnet and staurolite, suggesting syn-foliation breakdown of andalusite. Microstructural relationships suggest that garnet, staurolite, and andalusite formed before and possibly early in the foliation, and staurolite growth continued syn-foliation. Garnet exhibits core-to-rim decreasing xSps (10–1 %) and Fe# (92–90 %), a near-rim abrupt jump of xGrs (4 to 6 %) (Fig. DR2B). Staurolite composition is ZnO = 0.89–1.00 wt.% and Fe# = 85–87%, and biotite composition is Fe# = 59–61%.

Sample ROB1612 (S18°50.834’, E143°32.034’) was collected in the garnet–staurolite zone of the Robertson River Metamorphics, in the central Georgetown Inlier (Fig. DR1C). It is comprised of garnet (up to 2 mm across), staurolite (up to 1 cm long) and biotite (up to 1 mm long) porphyroblasts surrounded by a foliated matrix of biotite, muscovite, quartz, ilmenite, and accessory rutile, apatite, monazite, and tourmaline. Subhedral garnet is occasionally included in staurolite (Fig. 2C). Garnet exhibit sigmoidal inclusions trails that appear truncated by the matrix foliation. Staurolite present inclusions-free domains (possible initial nucleation sites) but is mostly poikilitic, with slightly curvilinear trails that are well continuous with the matrix foliation (Fig. 2C). The muscovite–biotite-defined matrix foliation wraps garnet and staurolite porphyroblasts, forming non- to moderately foliated strain shadows. Accordingly, microstructural relationships suggest that garnet and possibly early staurolite growth was essentially inter-tectonic and was followed by staurolite growth during the early development of the matrix foliation. Garnet exhibits rimward decreasing xSps (14–2 %), xGrs (17–13 %), and Fe# (=Fe^{2+}/[Fe^{2+}+Mg] = 93–90 %) (Fig. DR2C). Garnet outermost rim exhibits an xSps increase (8%) and Fe#, and a drop of xGrs (8%). Staurolite composition is Fe# =85–86 % and ZnO = 0.11–0.23 wt.%, which is significantly lower than in SCG1608. Matrix ilmenite was partially overgrown by rutile, and garnet occasionally replaced by plagioclase (An_{42}). Biotite (Fe# = 55–59 %) seems restricted to the matrix as it was not observed as inclusion in garnet or staurolite.

PRESSURE–TEMPERATURE EVOLUTION

Sample SCG1608

Garnet core. Nearly homogeneous Mn content observed in garnet core (Fig. DR2B) likely reflects that garnet inner core was not measured. Nevertheless, the grossular component (xGrs) is constant around 4% and Fe# was around 92%, so that P–T conditions at garnet growth initiation can be estimated by searching the intersection between these xGrs and Fe#. Thus, the equilibrium phase diagram obtained for SCG1608 non-fractionated, bulk-rock composition (Fig. DR3A) suggests that garnet started to form in the stability field of biotite + plagioclase + chlorite

± andalusite, at ~0.2 GPa, ca. 520–530°C, that is along an elevated thermal gradient (~70°C/km). We note that the calculation does not account for ZnO, which is significant (0.89–1.00 wt.%) in SCG1608 staurolite and might have extended its stability toward lower pressures. If the phase diagram is otherwise accurate, the predicted <4 vol.% of plagioclase would have been consumed during subsequent metamorphic stages.

Garnet rim. The equilibrium phase diagram obtained for the growth of garnet rim (Fig. DR3B) shows that, without MnO, garnet stability is restricted to pressures above 0.55 GPa. The observed compositions of garnet rim (Grs6; Fe# = 90 %) and staurolite (Fe# = 14–16 %) are best approached at 0.6–0.65 GPa and 570–650°C. At these conditions, ilmenite is stable, in agreement with the lack of rutile overprint, and near the disappearance of plagioclase, which might be recorded by the Ca-jump observed at the garnet rim (Fig. DR2B). Kyanite previously reported to have overgrown andalusite but pre-dated sillimanite (Rubenach et al., 2008) is consistent with the pressure conditions in Figure DR3B.

Sample ROB1612

Garnet core. The equilibrium phase diagram calculated for the non-fractionated bulk-composition of sample ROB1612 (Fig. DR3C) predicts that pressures above 0.4 GPa are required for garnet to form before staurolite along a prograde path, as indicated by petrological observations. The observed composition of garnet core is reproduced at ~530°C, 0.6 GPa in the stability field of the assemblage garnet–chloritoid–chlorite–margarite–ilmenite–muscovite–quartz–water. In the calculated phase diagram, the co-stability of chloritoid and staurolite is restricted to a very small temperature range, implying that, during heating, chloritoid is completely replaced by staurolite. This is consistent with the field observation that both minerals are nearly never found in the same rock and the chloritoid-, and staurolite domains do essentially not overlap (Reinhardt and Rubenach, 1989). We infer the same applies to chlorite, which, for the modelled composition, is completely replaced by staurolite and biotite in the upper staurolite stability field. The prediction of small amounts of margarite is likely an artefact of the white-mica solid solution (White et al., 2001, 2007; White et al., 2014). Furthermore, above 550–570°C, margarite is replaced by plagioclase, which is occasionally observed in this sample. We therefore assume that the phase diagram and garnet compositional isopleths match our observations and garnet growth started from 0.6 GPa and 530°C.

Garnet rim. The equilibrium phase diagram obtained for the growth of garnet rim (Fig. DR3D) shows that, without MnO, garnet stability is restricted to pressures above 0.6 GPa. The observed compositions of garnet rim (Grs11; Fe# = 9) and staurolite (Fe# = 14–16) are best approached at >0.7 GPa and 570–590°C. At these conditions, rutile is stable as observed by the partial replacement of ilmenite. The prediction that biotite is not stable at this stage is in agreement with the lack of biotite inclusions in garnet and staurolite. The phase diagram suggests that biotite and plagioclase growth after garnet was associated with heat at peak pressure. The absence of sillimanite overprint on staurolite suggests that decompression below 0.5 GPa was accompanied by cooling.

DEEP-SEISMIC PROFILE

In Figure 4A, structural discontinuities identified by Korsch et al. (2012) on the Geoscience Australia deep-seismic reflection profile 07GA-IG1 were tectonically re-assessed on the basis of our new results. The crustal architecture of Korsch et al. (2012) was simplified, for the sake of readability, but not re-interpreted. The original seismic data and their interpretation are provided in Figure DR4; and details on seismic interpretation can be found in Korsch et al. (2012).

ADDITIONAL REFERENCES

Bizzarro, M., Baker, J. A., Haack, H., Ulfbeck, D., and Rosing, M., 2003, Early history of Earth's crust–mantle system inferred from hafnium isotopes in chondrites: Nature, v. 421, p. 931-933.

de Capitani, C., and Petrakakis, K., 2010, The computation of equilibrium assemblage diagrams with Theriak/Domino software: American Mineralogist, v. 95, no. 7, p. 1006-1016.

Droop, G., 1987, A general equation for estimating Fe3+ concentrations in ferromagnesian silicates and oxides from microprobe analyses, using stoichiometric criteria: Mineralogical magazine, v. 51, no. 361, p. 431-435.

Giles, D., Betts, P., Aillères, L., Hulscher, B., Hough, M., and Lister, G., 2006, Evolution of the Isan Orogeny at the southeastern margin of the Mt Isa Inlier: Australian Journal of Earth Sciences, v. 53, p. 91–108, https://doi.org/10.1080/08120090500432470.

Münker, C., Weyer, S., Scherer, E., and Mezger, K., 2001, Separation of high field strength elements (Nb, Ta, Zr, Hf) and Lu from rock samples for MC-ICPMS measurements: Geochemistry, Geophysics, Geosystems, v. 2, no. 12.

Pourteau, A., Scherer, E. E., Schorn, S., Bast, R., Schmidt, A., and Ebert, L., 2018, Thermal evolution of an ancient subduction interface revealed by Lu–Hf garnet geochronology, Halilbağı Complex (Anatolia): Geoscience Frontiers.

Reinhardt, J., and Rubenach, M., 1989, Temperature-time relationships across metamorphic zones: evidence from porphyroblast—matrix relationships in progressively deformed metapelites: Tectonophysics, v. 158, no. 1-4, p. 141-161.

Rubenach, M. J., Foster, D., Evins, P., Blake, K., and Fanning, C., 2008, Age constraints on the tectonothermal evolution of the Selwyn Zone, Eastern fold belt, Mount Isa Inlier: Precambrian Research, v. 163, no. 1, p. 81-107.

Scherer, E., Münker, C., and Mezger, K., 2001, Calibration of the lutetium-hafnium clock: Science, v. 293, no. 5530, p. 683-687.

Smit, M. A., Scherer, E. E., Bröcker, M., and van Roermund, H. L. M., 2010, Timing of eclogite facies metamorphism in the southernmost Scandinavian Caledonides by Lu-Hf and Sm-Nd geochronology: Contributions to Mineralogy and Petrology, v. 159, no. 4, p. 521-539.

Söderlund, U., Patchett, P. J., Vervoort, J. D., and Isachsen, C. E., 2004, The 176 Lu decay constant determined by Lu–Hf and U–Pb isotope systematics of Precambrian mafic intrusions: Earth and Planetary Science Letters, v. 219, no. 3, p. 311-324.

Vervoort, J. D., Patchett, P. J., Söderlund, U., and Baker, M., 2004, Isotopic composition of Yb and the determination of Lu concentrations and Lu/Hf ratios by isotope dilution using MC-ICPMS: Geochemistry, Geophysics, Geosystems, v. 5, no. 11.

White, R., Powell, R., and Holland, T., 2001, Calculation of partial melting equilibria in the system Na2O–CaO–K2O–FeO–MgO–Al2O3–SiO2–H2O (NCKFMASH): Journal of metamorphic Geology, v. 19, no. 2, p. 139-153.

White, R., Powell, R., and Holland, T., 2007, Progress relating to calculation of partial melting equilibria for metapelites: Journal of metamorphic Geology, v. 25, no. 5, p. 511-527.
White, R., Powell, R., Holland, T., Johnson, T., and Green, E., 2014, New mineral activity–composition relations for thermodynamic calculations in metapelitic systems: Journal of Metamorphic Geology, v. 32, no. 3, p. 261-286.
Whitney, D. L., and Evans, B. W., 2010, Abbreviations for names of rock-forming minerals: American mineralogist, v. 95, no. 1, p. 185-187.
Withnall, I.W., and Hutton, L.J., 2013, Proterozoic—North Australian Craton, *in* Jell, P. A., ed., Geology of Queensland: Brisbane, Queensland, Geological Survey of Queensland, p. 23–111.

FIGURE CAPTIONS

Table DR1. Lu and Hf isotope data for the investigated samples.

Table DR2. Modeled bulk-rock compositions for samples SCG1608 and ROB1612.

Figure DR1. A: Simplified geological map of Proterozoic northeast Australia. Yellow boxes encompass the study areas, shown in B and C. The discontinuous black line, 'Tasman Line', depicts the eastern edge of Proterozoic Australia. B: Geological map of the easternmost Mount Isa Inlier (representing the Paleoproterozoic North Australian margin). C: Geological map of the central Georgetown Inlier (representing part of Paleoproterozoic Laurentia).

Figure DR2. Rim–core–rim compositional profiles of garnets from the study samples, expressed as proportions in pure end-members and Fe# (=$Fe^{2+}/(Fe^{2+}+Mg)$).

Figure DR3. Equilibrium phase diagrams calculated for samples SCG1608 (Mount Isa Inlier) and ROB1612 (Georgetown Inlier) using the bulk-rock MnNCKFMASHT compositions, suitable for modelling garnet core (A and C); and bulk-rock NCKFMASHT compositions fractionated for garnet growth, suitable for modelling essentially-Mn-free garnet rim (B and D). Modelled bulk-rock compositions are given in Table DR2.

Figure DR4. Geoscience Australia deep-seismic reflection profile 07GA-IG1 from the Mount Isa Inlier to the Georgetown Inlier. A: Uninterpreted line (as in Korsch et al., 2012); B: interpreted line (Korsch et al., 2012); C: tectonic re-assessed crustal architecture (this study).

Table DR1. Lu and Hf isotope data for the investigated samples.

Aliquot	Lu (ppm)	Hf (ppm)	$^{176}Lu/^{177}Hf^{c}$	$^{176}Hf/^{177}Hf^{c}$	Lu–Hf age (Ma)	$^{176}Hf/^{177}Hf_0^{c}$	MSWD
Sample: ROB1612 (Georgetown)							
Grt-1	8.51	3.54	0.3404(9)	0.291655(41)			
Grt-2	9.43	3.26	0.4102(10)	0.293752(49)			
Grt-3	8.22	3.64	0.3206(8)	0.291010(43)			
matrix-1[a]	0.402	5.11	0.01116(3)	0.281665(25)			
					1597.9 ± 5.8	0.281327(25)	0.87
Sample: SCG1603 (Mount Isa)							
Grt-1	13.3	0.963	1.961(5)	0.341244(51)			
Grt-2	11.6	0.943	1.745(4)	0.334684(53)			
Grt-3	13	1.1	1.665(4)	0.332077(50)			
matrix-1[b]	0.223	5.75	0.005507(14)	0.281654(21)			
matrix-2[a]	0.181	5.1	0.005021(13)	0.281644(20)			
					1606.5 ± 2.4	0.281489(14)	1.3
Sample: SCG1608 (Mount Isa)							
Grt-1	7.72	3.11	0.3522(9)	0.292068(39)			
Grt-2	8.15	3.29	0.3515(9)	0.292041(43)			
Grt-3	8.75	3.32	0.3737(9)	0.292676(40)			
matrix-1[b]	0.159	6.35	0.003548(9)	0.281457(20)			
matrix-2[a]	0.0712	4.78	0.002113(5)	0.281404(18)			
					1603.9 ± 4.5	0.281344(13)	0.86

[a]Table-top dissolution

[b]Autoclave dissolution

[c]Number in brackets denotes the uncertainty in the least significant digit(s)

Table DR2. Modeled bulk-rock compositions for samples *SCG1608* and *ROB1612*.

		SCG1608 (Mount Isa) garnet–andalusite–staurolite schist		*ROB1612 (Georgetown)* garnet–staurolite schist	
		Non-fractioned	Fractionated	Non-fractioned	Fractionated
		Fig. DR3A	Fig. DR3B	Fig. DR3C	Fig. DR3D
mol%	SiO2	73.12	74.03	72.81	74.46
	TiO2	0.59	0.6	0.61	0.64
	Al2O3	11.39	11.31	13.29	13.23
	FeO	7.37	6.32	5.85	4.42
	MnO	0.11	0	0.12	0
	MgO	3.62	3.61	3.67	3.71
	CaO	0	0.21	0.48	0.19
	Na2O	0.59	0.6	0.43	0.45
	K2O	3.21	3.3	2.74	2.89
	H2O	*excess*	*excess*	*excess*	*excess*

Figure DR1

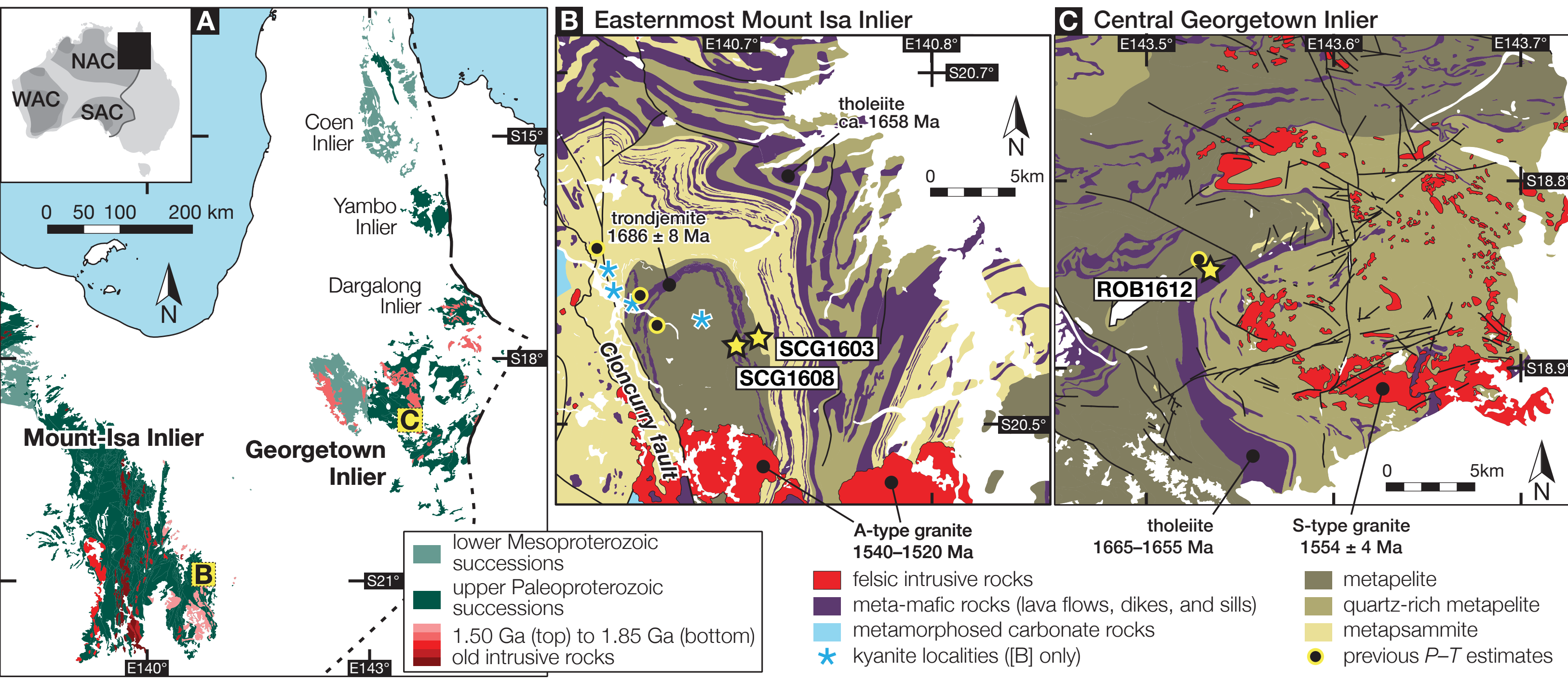
A
NAC
WAC
SAC
0 50 100 200 km
N
Coen Inlier
Yambo Inlier
Dargalong Inlier
S15°
S18°
S21°
E140°
E143°
Mount-Isa Inlier
Georgetown Inlier
C
B
lower Mesoproterozoic successions
upper Paleoproterozoic successions
1.50 Ga (top) to 1.85 Ga (bottom) old intrusive rocks
B Easternmost Mount Isa Inlier
E140.7°
E140.8°
S20.7°
S20.5°
tholeiite ca. 1658 Ma
0 5km
N
trondjemite 1686 ± 8 Ma
SCG1603
SCG1608
Cloncurry fault
A-type granite 1540–1520 Ma
C Central Georgetown Inlier
E143.5°
E143.6°
E143.7°
S18.8°
S18.9°
ROB1612
0 5km
N
tholeiite 1665–1655 Ma
S-type granite 1554 ± 4 Ma
felsic intrusive rocks
meta-mafic rocks (lava flows, dikes, and sills)
metamorphosed carbonate rocks
kyanite localities ([B] only)
metapelite
quartz-rich metapelite
metapsammite
previous P–T estimates

Figure DR2

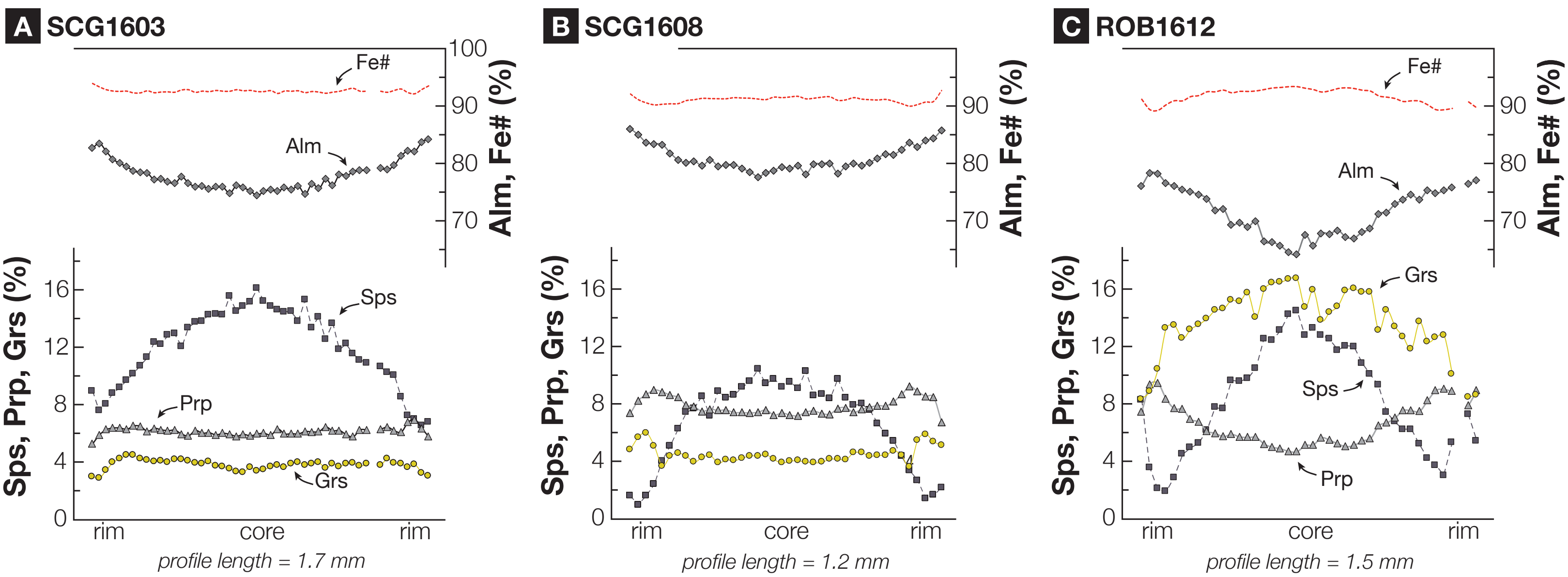
A SCG1603
B SCG1608
C ROB1612
Fe#
Alm
Sps
Prp
Grs
Alm, Fe# (%)
Sps, Prp, Grs (%)
100
90
80
70
16
12
8
4
0
rim
core
rim
profile length = 1.7 mm
profile length = 1.2 mm
profile length = 1.5 mm

Figure DR3

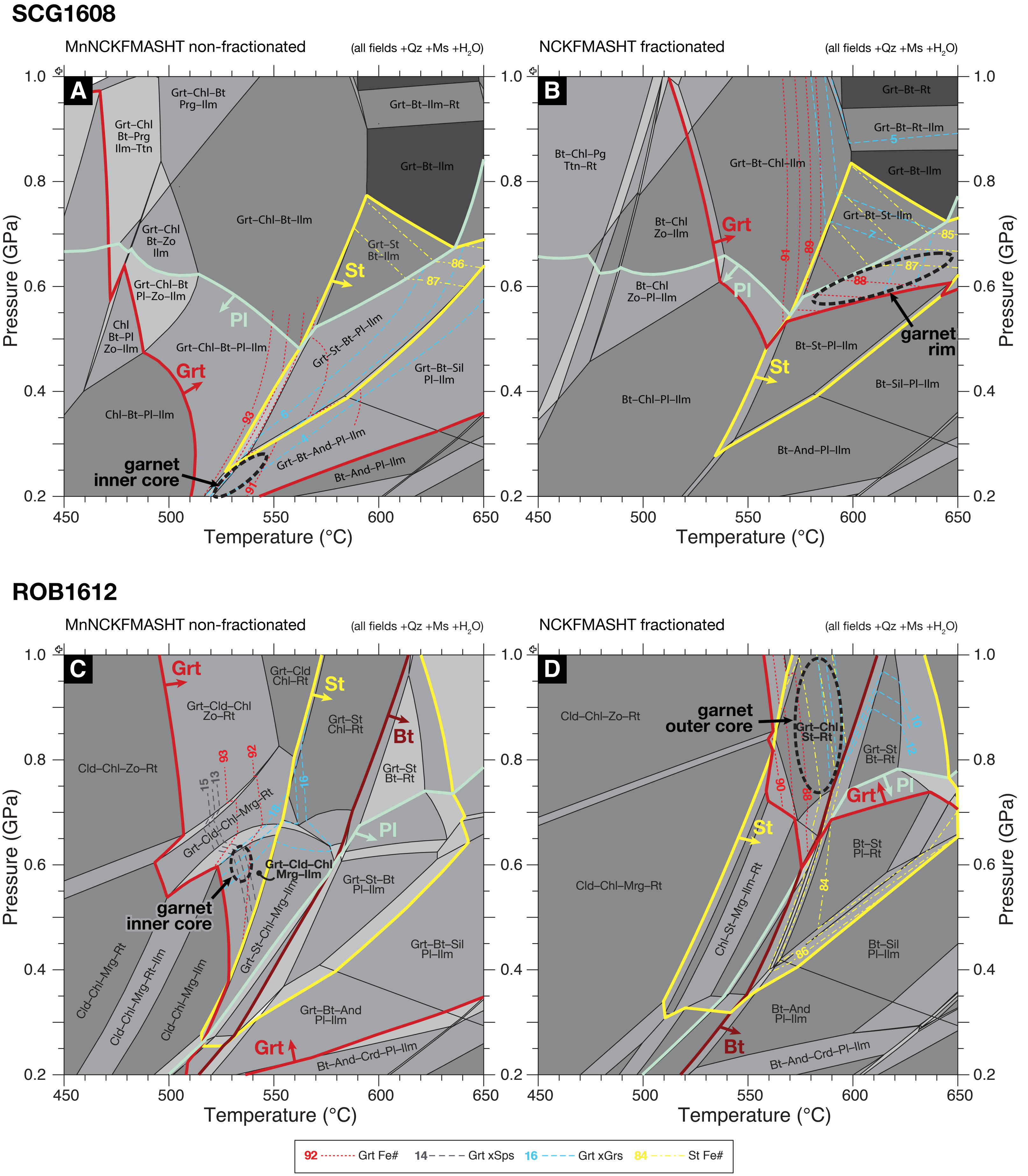

SCG1608
MnNCKFMASHT non-fractionated
(all fields +Qz +Ms +H2O)
NCKFMASHT fractionated
(all fields +Qz +Ms +H2O)
A
B
Pressure (GPa)
Temperature (°C)
garnet inner core
garnet rim
ROB1612
MnNCKFMASHT non-fractionated
(all fields +Qz +Ms +H2O)
NCKFMASHT fractionated
(all fields +Qz +Ms +H2O)
C
D
garnet inner core
garnet outer core
92 Grt Fe#
14 Grt xSps
16 Grt xGrs
84 St Fe#

Figure DR4

A Uninterpreted seismic profile 07GA-IG1 (as in Korsch et al., 2012, Fig. 3)

full-resolution seismic data available on http://www.ga.gov.au/

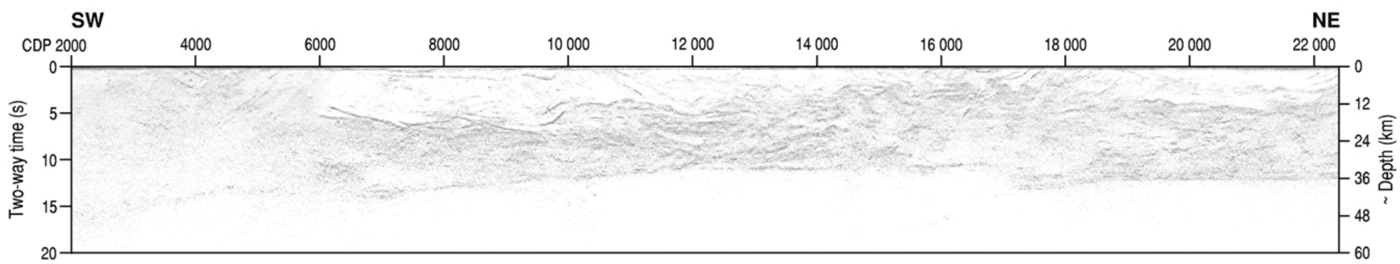

B Interpreted seismic profile 07GA-IG1 (Korsch et al., 2012, Fig. 3)

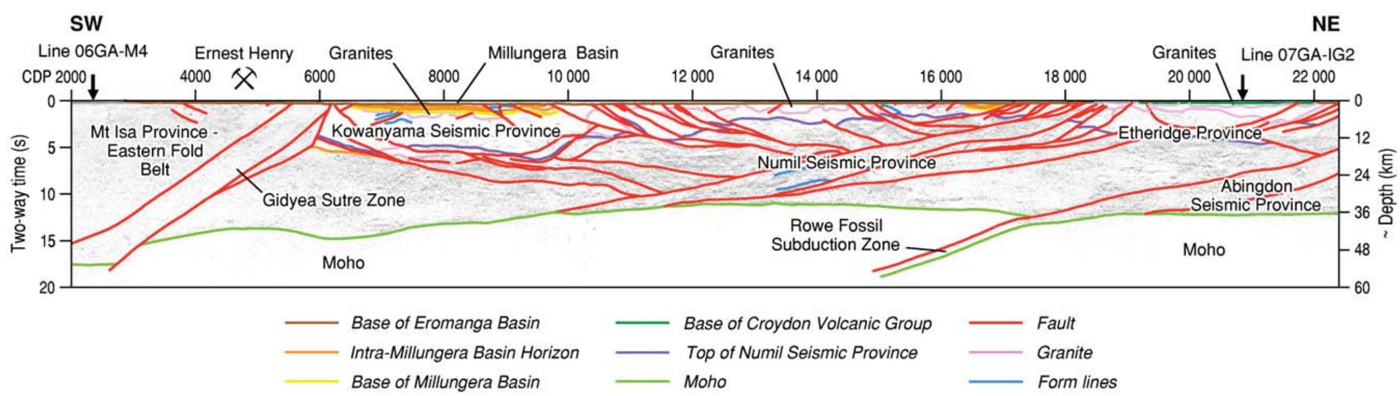

C Re-assessed tectonic architecture (this study, Fig. 4A)